

Angular distributions and quantum beats of photoelectrons from resonant two-photon ionization of lithium

Ring-ling Chien, Oliver C. Mullins, and R. Stephen Berry

Department of Chemistry and the James Franck Institute, The University of Chicago, Chicago, Illinois 60637

(Received 7 April 1983)

Angular distributions of photoelectrons from resonant two-photon ionization via the $2p\ ^2P_{1/2}$ or $2p\ ^2P_{3/2}$ state of lithium have been measured. The quantum beats of hyperfine levels strongly affect the angular distribution. Three microscopic parameters are extracted: the ratio of the radial matrix elements from $2p$ excited states to $l=0$ and 2 final states, the difference of the phase shifts of the continuum electrons in final channels, and a time-dependent parameter for hyperfine interaction. The experimental results agree with theoretical quantum-defect calculation and extrapolated bound-state data.

INTRODUCTION

The study of resonant multiphoton ionization can provide information concerning ground and excited states and the interaction of free electrons with atomic or molecular species.

Information available from measurements of total photoionization yields includes ionization potentials, transition probabilities to excited states, and total photoionization cross sections. Measurements of the angular distributions of photoelectrons, the subject of this paper, provide information concerning the transition amplitudes from bound excited states to the individual free partial waves, the difference in phase shifts of these partial waves, and some characteristics of the radiation fields causing the transitions. Additionally, pulsed excitations can be used to generate coherent superpositions in the intermediate states. An example occurs when pumping the hyperfine states of an atomic level. In this situation, the angular distribution is affected by the hyperfine splittings, the laser-pulse durations, and the time between excitation and ionization.

In the theoretical section of this report, the general form of the angular distribution of photoelectrons from resonant two-photon ionization is developed, based on that form of density-matrix formalism called the Liouville representation. The influence of hyperfine levels is also discussed.

In previous reports,^{1,2} the angular distribution of photoelectrons resulting from the resonant two-photon ionization of a sodium atomic beam was studied. In the experiment reported here, an analogous study was made of lithium. Lithium atoms were excited to the $2p\ ^2P_{3/2}$ or $2p\ ^2P_{1/2}$ state by linearly polarized light from a tunable-dye-laser pulse and then ionized by a pulse of linearly polarized light from a nitrogen laser. The angular distributions of photoelectrons were measured as functions of the angle between the two polarization directions, and as functions of the time interval between the two laser pulses. Three microscopic parameters are extracted from the data: the ratio of the radial matrix elements

$2p \rightarrow \epsilon s$ and $2p \rightarrow \epsilon d$, the difference of the s - and d -wave phase shifts, and a parameter associated with coherent pumping of the hyperfine levels.

REVIEW OF THEORY

For a resonant two-photon process involving a transition from initial states i to final states f , the differential cross section is proportional to

$$\sum_{i,f} \left| \sum_a \langle \psi_f | V_2 | \psi_a \rangle \langle \psi_a | V_1 | \psi_i \rangle \right|^2.$$

To avoid the complexity of summing over all the magnetic sublevels, it is convenient to use the density matrix and observable operator formalism known as the "Liouville representation."³ The theoretical method introduced to interpret our measurement of angular distributions of photoelectrons from resonant two-photon ionization of Na with hyperfine interaction^{1,2} is presented in this section. The method was previously outlined very briefly, but the following discussion develops it in enough detail to be used by others. By imposing symmetry constraints on the density operator and detector operator levels directly, the phenomenological equations can be derived in a particularly straightforward way.

The purpose of this section is to formulate the angular distributions of photoelectrons from resonant two-photon ionization of atoms using the irreducible Liouville representation. A related result, the distribution of spin polarization from two-photon ionization with hyperfine interactions, was derived in a related density-matrix formalism by Nienhuis *et al.*⁴ This formalism could be used to derive the present result but the explicit inclusion of the detector operator, as done here, makes the derivation and the final expressions more transparent. This is especially important as the complexity of the problems increases, for example, to molecular photoionization.

The density operator is expressed in the irreducible Liouville representation as a ket vector:

$$|\rho(t)\rangle_L = \sum_{\substack{j,j' \\ J,M}} |(jj')JM\rangle_L \langle (jj')JM | \rho(t) \rangle_L, \quad (1)$$

where

$$\begin{aligned} \langle (jj')JM | \rho(t) \rangle_L &= \sum_{m,m'} (-1)^{j'-m} \langle jmj' - m' | JM \rangle \langle jm | \rho(t) | j'm' \rangle, \\ & \quad (2) \end{aligned}$$

$$\begin{aligned} |(jj')JM\rangle_L &= \sum_{m,m'} (-1)^{j'-m} \langle jmj' - m' | JM \rangle |jm\rangle \langle j'm' |, \\ & \quad (3) \end{aligned}$$

and the subscript L of the ket refers to Liouville representation. The $\langle (jj')JM | \rho(t) \rangle_L$ amplitude of the $|(jj')JM\rangle_L$ basis vector is equivalent to Fano and Racah's definition⁵ of the statistical tensor $[(j|\rho(t)|j')]_M^J$. Equation (2) shows that a knowledge of the density matrix is entirely equivalent to a knowledge of the Liouville amplitude of the density operator.

Similarly, the observable \mathcal{E} may also be represented by a covector ${}_L\langle \mathcal{E} |$ with the components ${}_L\langle \mathcal{E} | (jj')JM \rangle$ in the ${}_L\langle (jj')JM |$ basis. The expectation value of the operator \mathcal{E} may then be viewed as a scalar product of two vectors $\mathcal{E} \cdot \bar{\rho}(t)$ or $\langle \mathcal{E} | \rho(t) \rangle_L$.

The time evolution of a density operator can be described by the equation³

$$|\rho(t)\rangle_L = e^{-iLt/\hbar} |\rho(0)\rangle_L = \mathcal{S} |\rho(0)\rangle_L, \quad (4)$$

where L is the Liouville operator and $\mathcal{S} = e^{-iLt/\hbar}$ is the

transition operator in Liouville representation.

From Eqs. (1) and (4) we obtain an expression for the expectation value of the observable

$$\begin{aligned} \langle \mathcal{E} \rangle &= \langle \mathcal{E} | \rho(t) \rangle_L \\ &= \sum_{\substack{j_i, j_i' \\ j_f, j_f' \\ J_i, M_i, J_f, M_f}} {}_L\langle \mathcal{E} | (j_f j_f') J_f M_f \rangle \\ & \quad \times \langle (j_f j_f') J_f M_f | \mathcal{S} | (j_i j_i') J_i M_i \rangle_L \\ & \quad \times \langle (j_i j_i') J_i M_i | \rho(0) \rangle_L. \end{aligned} \quad (5)$$

The computational advantage of the Liouville representation appears here: One obtains probabilities or intensities directly rather than amplitudes. This is especially important for simplifying problems with many coupled angular momenta. With suitable metrics, the spaces of observables and density states are distinct but dual to each other, conventional Racah algebra can be used, and a theorem, precisely analogous to the Wigner-Eckart theorem, holds for intensities just as the Wigner-Eckart theorem holds for the amplitudes.^{6,7}

The following discussion summarizes the theory of two-photon ionization in the Liouville representation in order to interpret the experiments described in the subsequent sections. Specifically, the expression for the angular distribution of electrons resulting from resonant two-photon ionization is derived.

From Eq. (5) and the Wigner-Eckart theorem, the angular distribution can be expressed as

$$\begin{aligned} \frac{d\sigma}{d\Omega} &= \sum_{\text{all}} {}_L\langle \mathcal{E}(\Omega) | (l_2 l_2') L_2, (s_2 s_2') S_2, (i_2 i_2') I_2; JM \rangle \\ & \quad \times \langle (l_2 l_2') L_2, (s_2 s_2') S_2, (i_2 i_2') I_2; J || \mathcal{S} || (i_a i_a) I_a, (j_a j_a) J_a, (11) P_1, (11) P_2; J \rangle_L \\ & \quad \times \langle (i_a i_a) I_a, (j_a j_a) J_a, (11) P_1, (11) P_2; JM | \rho(0) \rangle_L, \end{aligned} \quad (6)$$

where l_2 (l_2') and s_2 (s_2') are the orbital and spin angular momentum of the free electron, i_2 (i_2') is the angular momentum of the ionic core left, and i_a and j_a the initial nuclear spin and electron angular momenta, respectively. The dipole approximation is also assumed and P_1 and P_2 are the polarization moments (0 or 2 for linearly polarized light) of the first and second photon, respectively.

The Liouville amplitude describing an electron detector with unobserved nuclear and electron spin is given by⁷

$${}_L\langle \mathcal{E}(\Omega) | (l_2 l_2') L_2, (s_2 s_2') S_2, (i_2 i_2') I_2 s JM \rangle = (4\pi)^2 (-1)^{l_2} \left[\frac{(2l_2+1)(2l_2'+1)}{4\pi} \right]^{1/2} \begin{bmatrix} l_2 & l_2' & L_2 \\ 0 & 0 & 0 \end{bmatrix} Y_{L_2 M}(\Omega) \delta_{S_2 0} \delta_{I_2 0} \delta_{L_2 J}. \quad (7)$$

The Liouville amplitude describing two different polarized photons and an isotropic atomic state is given by

$$\begin{aligned} \langle (i_a i_a) I_a, (j_a j_a) J_a, (11) P_1, (11) P_2; JM | \rho(0) \rangle_L \\ = \sum_{m_1, m_2} [(2j_a+1)(2i_a+1)]^{-1/2} \langle (11) P_1 m_1 | \rho_{P_1} \rangle_L \langle (11) P_2 m_2 | \rho_{P_2} \rangle_L \langle P_1 m_1 P_2 m_2 | JM \rangle. \end{aligned} \quad (8)$$

The irreducible component of the photon state $\langle (11) P m | \rho_P \rangle_L$ can be calculated from Eq. (2) if the ellipticity and the polarization direction of the light beam are known.^{8,9}

For this two-photon process the reduced transition matrix of Eq. (6) can be decomposed into three parts: ionization \mathcal{S}_2 , hyperfine interaction \mathcal{S}_{hf} , and excitation \mathcal{S}_1 . Thus

$$\begin{aligned} & \langle (l_2 l_2') L_2, (ss) 0, (i_2 i_2) 0; L_2 | | \mathcal{S} | | (i_a i_a) 0, (j_a j_a) 0, (11) P_1, (11) P_2; J \rangle_L \\ &= \langle (l_2 l_2') L_2, (ss) 0, (i_2 i_2) 0; L_2 | | \mathcal{S}_2 | | (j_1 j_1) J_1, (i_1 i_1) 0 (11) P_2; L_2 \rangle_L \langle (i_1 i_1) 0, (j_1 j_1) J_1; F_1 | | \mathcal{S}_{\text{hf}} | | (i_1 i_1) 0, (j_1 j_1') J_1; F_1 \rangle_L \\ & \quad \times \langle (i_1 i_1) 0, (j_1 j_1) J_1; F_1 | | \mathcal{S}_1 | | (i_a i_a) 0, (j_a j_a) 0, (11) P_1; P_1 \rangle \delta_{J_1 F_1} \delta_{i_1 i_2} \delta_{P_1 F_1} \\ &= [P_2, l_2, l_2']^{1/2} [J_1]^{3/2} [j_1]^2 \begin{pmatrix} s & s & 0 \\ l_1 & l_1 & J_1 \\ j_1 & j_1 & J_1 \end{pmatrix} \begin{pmatrix} l_1 & 1 & l_2 \\ l_1 & 1 & l_2' \\ J_1 & P_2 & L_2 \end{pmatrix} \begin{pmatrix} j_a & 1 & j_1 \\ j_a & 1 & j_1 \\ 0 & P_1 & J_1 \end{pmatrix} \\ & \quad \times W(J_1, t) \langle j_1 || r_1 || j_0, 1; j_1 \rangle \langle j_0, 1; j_2 || r_2^\dagger || j_1 \rangle \langle l_2 || r_2 || l_2, 1; l_2 \rangle \langle l_1, 1; l_2' || r_2^\dagger || l_2' \rangle, \end{aligned} \quad (9)$$

where $[j] = (2j + 1)$ and $\langle j' || r || j, l; j' \rangle$ is the reduced transition matrix in Hilbert space.

The time-dependent parameter $W(j_1, t)$ has the following expression:

$$W(J_1, t) = \sum_{f, f'} [J_1, f, f'] \begin{pmatrix} j_1 & j_1 & J_1 \\ i & i & 0 \\ f & f' & J_1 \end{pmatrix}^2 e^{-i\omega_{ff'} t - \Gamma t}, \quad (10)$$

where f is the total angular momentum and Γ is the lifetime of the excited state.

Thus, the density-matrix elements connecting different hyperfine levels precess with angular frequency $\omega_{ff'} = (E_f - E_{f'})/\hbar$ between excitation and ionization, where E_f and $E_{f'}$ are the energies of hyperfine levels with total angular momentum f and f' , respectively. If the durations of the light pulses are not negligible compared to the precessional periods $2\pi/\omega_{ff'}$, the effects of time evolution must be constructed by suitable convolutions of $W(j, t)$ [Eq. (10)] with the intensity profiles $I(t_1)$ and $I(t_2)$ of both laser pulses. The resulting functions

$$\chi(J_1, t) = \int_{-\infty}^{\infty} dt_2 \int_{-\infty}^{t_2} dt_1 W(J_1, t_2 - t_1) I(t_1) I(t_2) \quad (11)$$

become key quantities that can be computed from theory or treated as phenomenological parameters.

In the experiments described in the next section, atomic lithium $2s^2 S_{1/2}$ was resonantly excited to the $2p^2 P_{3/2}$ or $2p^2 P_{1/2}$ state and then photoionized. The laser beams were collinear and linearly polarized with an adjustable angle η between the polarization directions. For convenience the photon propagation direction is defined as the y axis and the polarization direction of the ionizing photon is defined as the z axis (see Fig. 1), so θ is the colatitude with respect to the axis of polarization of that photon.

The intensity of the electron signal in the (θ, ϕ) direction assumes the general form

$$\begin{aligned} \frac{d\sigma}{d\Omega} &\propto C_{00} P_{00}(\cos\theta) + C_{20} P_{20}(\cos\theta) + C_{21} P_{21}(\cos\theta) \cos\phi \\ & \quad + C_{22} P_{22}(\cos\theta) \cos 2\phi + C_{40} P_{40}(\cos\theta) \\ & \quad + C_{41} P_{41}(\cos\theta) \cos\phi + C_{42} P_{42}(\cos\theta) \cos 2\phi, \end{aligned} \quad (12)$$

where $P_{LM}(\cos\theta)$ is the associated Legendre function. The coefficient C_{LM} can be expressed in terms of the microscopic parameters, thus,

$$\begin{aligned} C_{00} &= \frac{1}{9} \{ [2\chi(0, t) + (2 - 3 \sin^2 \eta) \chi(2, t)] d_0^2 \\ & \quad + [4\chi(0, t) + \frac{1}{5} (2 - 3 \sin^2 \eta) \chi(2, t)] d_2^2 \}, \\ C_{20} &= \frac{2}{9} \{ [-4\chi(0, t) + 2(\sin^2 \eta - 2) \chi(2, t)] \\ & \quad \times d_0 d_2 \cos(\delta_0 - \delta_2) \\ & \quad + [2\chi(0, t) + (\frac{5}{7} - \frac{15}{14} \sin^2 \eta) \chi(2, t)] d_2^2 \}, \\ C_{21} &= \frac{1}{3} [-d_0 d_2 \cos(\delta_0 - \delta_2) + \frac{2}{7} d_2^2] \chi(2, t) \sin(2\eta), \\ C_{22} &= \frac{1}{6} (\frac{3}{7} d_2^2 \sin^2 \eta) \chi(2, t), \\ C_{40} &= \frac{12}{35} (2 - 3 \sin^2 \eta) d_2^2 \chi(2, t), \\ C_{41} &= \frac{6}{35} \sin(2\eta) d_2^2 \chi(2, t), \\ C_{42} &= \frac{1}{35} \sin^2 \eta d_2^2 \chi(2, t), \end{aligned}$$

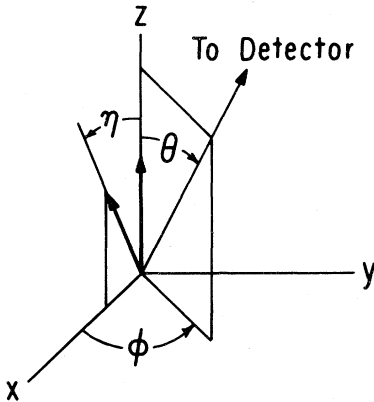


FIG. 1. System geometry. Electron trajectory is defined by θ and ϕ . Second photon polarization axis defines the z axis. Axis of the first photon polarization lies in the x - z plane at an angle η from the z axis. Lithium beam traverses the x axis.

where, as previously described, the $\chi(J_1, t)$ factors are time dependent and account for the hyperfine interaction in the intermediate state. The d_l and δ_l factors for the l th partial wave correspond to the dipole radial matrix element and the phase shift, respectively.

If the measurement is confined to the plane perpendicular to the propagation direction of the light ($\phi=0, \pi$), the general form Eq. (12) can be reduced to only five independent functions.¹

A special case results when the $2p^2P_{1/2}$ state is pumped with linearly polarized photons. The intermediate state ($^2P_{1/2}$) is isotropic so the resulting two-photon ionization expression reduces to the same form as the one-photon case:

$$\frac{d\sigma}{d\Omega} \propto (d_0^2 + 2d_2^2)P_{00}(\cos\theta) + 2[d_2^2 - 2d_0d_2\cos(\delta_0 - \delta_2)]P_{20}(\cos\theta).$$

EXPERIMENTAL

The general feature of the apparatus used to measure the angular distribution of photoelectrons has been previously described,¹ although some modifications have been made for the experiments with lithium. In particular, the energy of the photoelectrons from lithium $2p^2P$ is much lower than those from sodium $3p^2P$ with the same 3371-Å ionizing radiation, so it is more difficult to preserve linear trajectories of the photoelectrons from lithium.

An NRG nitrogen laser triggered at 60 Hz was used in this experiment. Part of the nitrogen laser beam pumped a dye laser tuned to the desired lithium excited state, and the other part of the nitrogen laser beam was adjusted to the desired time delay and then used to ionize the excited atom. Each laser beam passed through its own linear polarizer and moving polarization rotator. The collinear, linearly polarized beams intersected the atomic lithium beam inside the vacuum chamber.

For the nitrogen laser beam the polarizer is a calcite prism and the half-wave device is a quartz half-wave plate cut specifically for 3371 Å. For the dye laser beam the polarizer is a Wollaston prism and the half-wave device is a quartz Fresnel rhomb. Each half-wave device is in a rotating mount driven by motors synchronized to line frequency; the half-wave devices rotate at 1.5 Hz so that the axis of polarization of the linearly polarized light rotates at 3 Hz. Thus, with a fixed detector, the angular distribution of photoelectrons at ten different angles, each channel differing by 18° from the one preceding it, can be collected six times per second.

The photoelectrons were detected by a Galileo channeltron electron multiplier in the plane perpendicular to the propagation direction of the light and containing the collision region (i.e., $\phi=0$). The electron counts were accepted only during a gated window of 50-nsec duration and were stored into a CAMAC input register. The data were then collected by a Nova 1220 minicomputer.

The homemade dye laser has a resolution of about 0.5 Å at 6710 Å and the fine-structure splitting of the $2p P_{1/2}$ and $P_{3/2}$ levels of lithium is 0.15 Å. To pump only one of the fine-structure levels, a coated, 2.5-mm-thick etalon

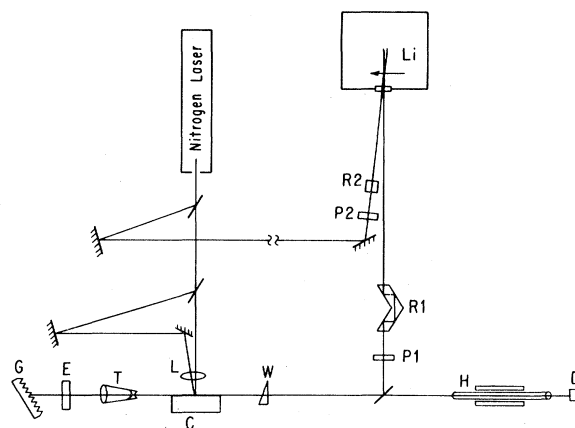


FIG. 2. Schematic of the laser system. G, grating; E, etalon; T, telescope; L, cylindrical lens; C, dye cavity; W, wedge prism; H, heat pipe; D, photodiode; P1, P2, polarizers; R1, half-wave Fresnel rhomb; R2, half-wave plate.

with 87% reflection at 6710 Å was used. The resolution with the etalon is approximately 0.05 Å. To increase the dye-laser output power, a Hänsch design¹⁰ with an oscillator and amplifier in a single cavity was employed as is schematically depicted in Fig. 2.

The dye used was DCM in dimethyl sulfoxide and the concentration of $\sim 1.0 \times 10^{-2} M$ was used to obtain maximum lasing power. A wickless lithium heat-pipe oven filled with 50 Torr of argon acted as an absorption cell for tuning the dye laser to the resonance absorption frequency.

The laser-beam—lithium-beam interaction region was located at the center of two concentric copper spheres in which screen-covered bands allowed photoelectron penetration. The potential of the inner copper sphere was maintained at ~ -50 V relative to the grounded outer sphere, so the signal electrons were accelerated but maintained their linear trajectories. The channeltron electron multiplier subtended a solid angle of $\sim 2.6 \times 10^{-3}$ sr. In front of the electron detector a small screen biased at -15 V eliminated spurious electrons. The copper spheres were cleaned with dilute HCl before each run to reduce the stray electric fields from surface charge buildup.

To preserve the linear trajectory of the slow photoelectrons, the entire apparatus is surrounded by three sets of Helmholtz coils which reduce the magnetic field to a few milligauss at the interaction region. At this level, the 0.13-eV electrons experience less than 2° deflection, due to magnetic fields, along their trajectories to the electron amplifier.

The channeltron counting system saturates at 60 counts/sec, so the count rate was kept ~ 5 counts/sec to minimize saturation effects which, additionally, were accounted for in the data reduction. At this count rate typical signal-to-background ratios were about 100:1 and each measurement took 3–4 hours. Replicate experiments were performed on different days, with fresh oven charges, to ensure the reliability of the data.

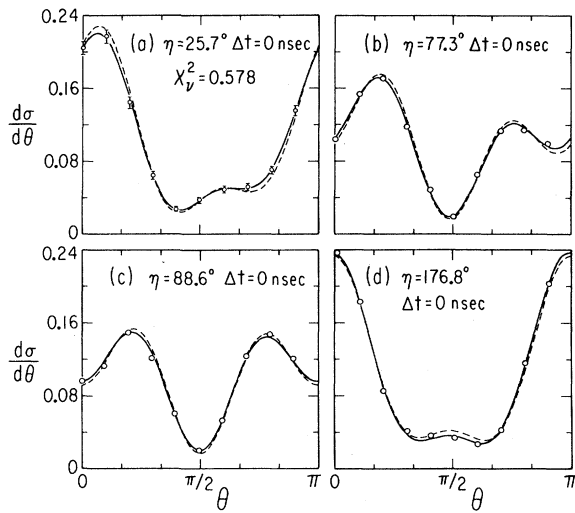


FIG. 3. Angular distributions of photoelectrons for coincidence pulses ($\Delta t=0$) with different η : (a) 25.7° , (b) 77.3° , (c) 88.6° , (d) 176.8° . Solid curves show least-squares fits of the measured angular distributions to Eq. (14). Scaling corresponds to the total number of experimental counts—the sum of the experimental peaks—being set to 1. Dashed curves represent the angular distributions expected from the average values of the microscopic parameters. (a) Shows the uncertainties of the data points (statistic $\chi^2_\nu=0.578$) which is typical for all of the experimental data.

DATA ANALYSIS

Each angular distribution measured as described above was corrected for background and fit by a nonlinear least-squares method to Eq. (12). Typical experimental data and least-squares fits are shown in Figs. 3 and 4, the solid lines represent least-squares fits to the individual angular distribution while the dashed lines represent simulations computed from the average experimental values determined from all of the experimental runs.

Our experimentally determined values for the difference in the phase shifts and the ratio of radial matrix elements are

$$\cos(\delta_0 - \delta_2) = -0.38 \pm 0.04,$$

$$d_0/d_2 = 0.43 \pm 0.15.$$

The experimental results for roughly the same polarization angle η with different time delays are shown in Fig. 4. The mean values of $\chi(2)/\chi(0)$ for the time delays between the laser pulses are (in nsec)

$$\chi(2)/\chi(0) = 0.84 \pm 0.07 \text{ at } \Delta t \sim 0$$

$$= 0.57 \pm 0.05 \text{ at } \Delta t \sim 20$$

$$= -0.073 \pm 0.020 \text{ at } \Delta t \sim 40.$$

The time variation of $\chi(2)/\chi(0)$ is shown in Fig. 5.

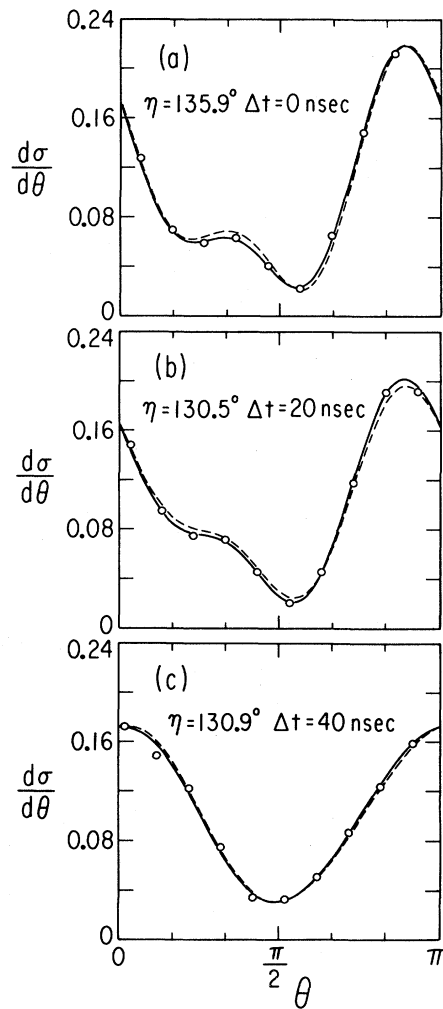


FIG. 4. Angular distributions of photoelectrons for roughly the same angle η with different time delays. (A) $\eta=135.9^\circ$, $\Delta t=0$ nsec; (b) $\eta=130.5^\circ$, $\Delta t=20$ nsec; (c) $\eta=130.9^\circ$, $\Delta t=40$ nsec. (See Fig. 3).

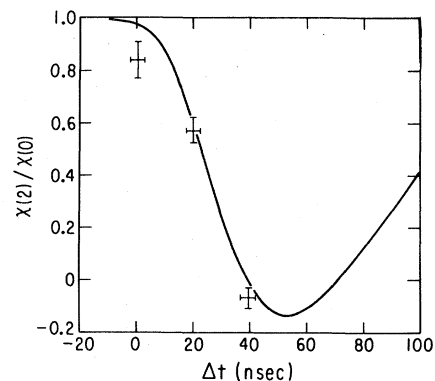


FIG. 5. Theoretical curve for $\chi(2)/\chi(0)$ with the experimental values for three different time delays.

DISCUSSION

The phase shift in the continuum wave of the (0.134-eV) photoelectrons and the ratio of radial matrix elements connecting the $2p$ excited state and the s and d continuum states have been directly measured. In addition, the effect of the hyperfine interaction on the angular distribution of photoelectrons has been observed. Naturally, we wish to compare the results with theoretical predictions.

From the quantum-defect theory,¹¹ the total phase shift δ_l for a continuum wave is given by a combination of a long-range Coulomb phase shift and the more interesting short-range phase shift:

$$\delta_l = \arg\Gamma(l+1-i/k) + \pi\mu_l(\epsilon),$$

where k is the electron's momentum in atomic units and $\mu_l(\epsilon)$ is the extrapolated quantum defect which is practically constant for electron energies near threshold. From bound-state data,¹² one expects $\mu_0=0.400$ and $\mu_2=0.00192$, leading to $\delta_0-\delta_2=4.097$ for the 0.134-eV photoelectrons. Also theoretical predictions¹³ of μ_0 and μ_2 at threshold indicate a value of $\delta_0-\delta_2$ between 4.083 and 4.287. These results are in agreement with our experimental value of 4.32 ± 0.04 .

The ratio of the radial matrix elements d_0/d_2 is related to the ratio of the partial cross sections σ_0/σ_2 as follows:

$$\sigma_0/\sigma_2 = \frac{1}{2}(d_0/d_2)^2.$$

From the calculations of Aymar *et al.*¹⁴ we infer a ratio of cross sections to be approximately 0.11 which gives for d_0/d_2 a value of 0.47 in agreement with our experimental value of 0.43 ± 0.15 . In spite of its rather substantial uncertainty, our value of d_0/d_2 is consistent with the assignment by Aymar *et al.* of the total cross section of ionization of the lithium $2p$ state as being largely hydrogenic in character.

The theoretical curve for $\chi(2)/\chi(0)$ shown in Fig. 5 was obtained from Eq. (10) by assuming Gaussian time profiles for the laser pulses and by using the reported value¹⁵ of the hyperfine splitting constant for ${}^7\text{Li}$, $a_{3/2} = -3.055$ MHz and $b_{\text{quad}} = -0.221$ MHz. Also considered was the effect of the natural abundance (7.42%) of ${}^6\text{Li}$ using a suitably scaled value of $a_{3/2}$. Assuming a mixture, we compute values of $\chi(2)/\chi(0)$ of 0.975, 0.584, and -0.0144 for the delays, 0, 20, and 40 nsec, respectively. The resulting agreement between the experimental results and theoretical values is excellent. The small discrepancy for the delay of 0 nsec may be due to deviation from the Gaussian shape of the laser pulses. The value of $\chi(2)/\chi(0)$ is especially sensitive to pulse shape for coincident pulses.

ACKNOWLEDGMENT

This research was supported initially by a grant from the National Science Foundation and completed with the support of a grant from the U.S. Department of Energy.

APPENDIX

In this appendix we list several equations involved in the Liouville representation.

The time evolution of a density operator can be written as

$$\begin{aligned} \rho(t) &= e^{-iHt}\rho(0)e^{iHt} \\ &= R\rho(0)R^\dagger. \end{aligned}$$

Comparing this with Eq. (4), one obtains

$$\mathcal{S}\rho(0) = R\rho(0)R^\dagger.$$

From Eqs. (1)–(4), the transition matrix has the form

$$\begin{aligned} \langle (j_f j_f') J_f M_f | \mathcal{S} | (j_i j_i') J_i M_i \rangle_L \\ = \sum_{\substack{m_i, m_i' \\ m_f, m_f'}} (-1)^{j_f' - m_f' - j_i' + m_i'} \langle j_f m_f j_f' - m_f' | J_f M_f \rangle \langle J_i M_i | j_i m_i j_i' - m_i' \rangle \langle j_f m_f | R | j_i m_i \rangle \langle j_i' m_i' | R^\dagger | j_f' m_f' \rangle. \end{aligned} \quad (\text{A1})$$

Since R is a scalar operator, it is diagonal in j and m ; hence we may use the Wigner-Eckert theorem to write

$$\langle j_f m_f | R | j_i m_i \rangle = \langle j_f || R || j_i \rangle \delta_{j_i j_f} \delta_{m_i m_f}, \quad (\text{A2})$$

where the scalar quantity $\langle j_f || R || j_i \rangle$ is called the reduced matrix element of R .

Substituting Eq. (A2) into (A1) we obtain a theorem in Liouville representation precisely analogous to the Wigner-Eckert theorem in Dirac representation:

$$\langle (j_f j_f') J_f M_f | \mathcal{S} | (j_i j_i') J_i M_i \rangle_L = \langle j_f || R || j_i \rangle \langle j_i' || R^\dagger || j_f' \rangle \delta_{J_i J_f} \delta_{M_i M_f} \delta_{j_i j_f} \delta_{j_i' j_f'} = \langle (j_f j_f') J_f || \mathcal{S} || (j_i j_i') J_i \rangle_L \delta_{j_i j_f} \delta_{j_i' j_f'} \delta_{J_i J_f}. \quad (\text{A3})$$

Similarly, the scalar quantity $\langle (j j') J || \mathcal{S} || (j j') J \rangle_L$ is called the reduced matrix element of \mathcal{S} in the Liouville representation.

Finally, one other equation used in this paper is the separation and expansion of the reduced matrix element in irreducible tensors:

$$\begin{aligned}
\langle (j_c j'_c) J_c || \mathcal{S} || (j_a j'_a) J_a, (j_b j'_b) J_b; J_c \rangle_L &= \langle (j_c j'_c) J_c || \mathcal{S} || ((j_a j'_b) j_c, (j'_a j'_b) j'_c) J_c \rangle_L ((j_a j_b) j_c, (j'_a j'_b) j'_c; J_c | (j_a j'_a) J_a, (j_b j'_b) J_b; J_c) \\
&= \langle j_c || R || j_a j_b; j_c \rangle \langle j'_a j'_b; j'_c || R^\dagger || j'_c \rangle [j_c j'_c J_a J_b]^{1/2} \begin{pmatrix} j_a & j_b & j_c \\ j'_a & j'_b & j'_c \\ J_a & J_b & J_c \end{pmatrix}. \quad (\text{A4})
\end{aligned}$$

-
- ¹J. C. Hansen, J. A. Duncanson, Jr., R.-L. Chien, and R. S. Berry, *Phys. Rev. A* **21**, 222 (1980).
- ²(a) M. P. Strand, J. C. Hansen, R.-L. Chien, and R. S. Berry, *Chem. Phys. Lett.* **59**, 205 (1978); (b) G. Leuchs, S. J. Smith, E. Khawaja, and H. Walther, *Opt. Comm.* **31**, 313 (1979).
- ³U. Fano, *Rev. Mod. Phys.* **21**, 74 (1957).
- ⁴G. Nienhuis, E. H. A. Granneman, and M. J. van der Wiel, *J. Phys. B* **11**, 1203 (1978).
- ⁵U. Fano and G. Racah *Irreducible Tensorial Sets* (Academic, New York, 1959).
- ⁶M. P. Strand and R. S. Berry, *J. Math. Phys.* **23**, 587 (1982).
- ⁷M. P. Strand, Ph.D. Thesis, University of Chicago, 1979 (unpublished).
- ⁸R.-L. Chien, Ph.D. Thesis, University of Chicago, 1983 (unpublished).
- ⁹J. C. Hansen, Ph.D. Thesis, University of Chicago, 1980 (unpublished); J. C. Hansen and R. S. Berry (unpublished).
- ¹⁰T. W. Hänsch, *Appl. Opt.* **11**, 895 (1972).
- ¹¹M. J. Seaton, *Mon. Not. R. Astron. Soc.* **118**, 504 (1958).
- ¹²I. Johansson, *Ark. Fys.* **15**, 169 (1958); P. d. P. Risberg, *ibid.* **10**, 583 (1956).
- ¹³C. Jaffé and W. P. Reinhardt, *J. Chem. Phys.* **66**, 1285 (1977).
- ¹⁴M. Aymar, E. Luc-Koenig, and F. Combet Farnoux, *J. Phys. B* **9**, 1279 (1976).
- ¹⁵H. Orth, H. Ackermann, and E. W. Otten, *Z. Phys. A* **273**, 221 (1975).